

bradscholars

Cavitation in die drawn poly(4-methyl-1-pentene) during second-stage tensile deformation

Item Type	Article
Authors	Han, C.;Lyu, D.;Lu, Y.;Caton-Rose, Philip D.;Coates, Philip;Men, Y.
Citation	Han C, Lyu D, Lu Y, et al (2024) Cavitation in die drawn poly(4-methyl-1-pentene) during second-stage tensile deformation. Polymer. 296: 126782
DOI	https://doi.org/10.1016/j.polymer.2024.126782
Rights	© 2024 Elsevier. This manuscript version is made available under the Creative Commons CC-BY-NC-ND license (https://creativecommons.org/licenses/by-nc-nd/4.0/)
Download date	2026-04-19 02:32:17
Link to Item	https://bradscholars.brad.ac.uk/handle/10454/20147.2

Cavitation in Die Drawn Poly(4-methyl-1-pentene) during Second-Stage Tensile
Deformation

Cenhui Han ^{a,b}, Dong Lyu ^{a,*}, Ying Lu ^a, Fin Caton-Rose ^c, Phil Coates ^c, Yongfeng Men ^{a,b,*}

^a *State Key Laboratory of Polymer Physics and Chemistry, Changchun Institute of Applied Chemistry, Chinese Academy of Sciences, Renmin Street 5625, Changchun 130022, PR China*

^b *School of Applied Chemistry and Engineering, University of Science and Technology of China, Hefei 230026, PR China*

^c *Polymer Interdisciplinary Research Centre, University of Bradford, Bradford BD7 1DP, U.K.*

Abstract

Pre-oriented poly(4-methyl-1-pentene) samples were prepared by the die drawing process. The stress whitening phenomenon induced by cavities in the different die drawn P4M1P samples during the second-stage tensile deformation was investigated at temperatures below and above T_g . At 30 °C and 50 °C, the cavitation process near the yield point is influenced by the fraction of unoriented crystal phase in pre-oriented samples. Cavities originate from the fracture of the crystalline skeleton at small strains were observed in the sample with a high fraction of unoriented crystalline phase. At high deformation temperature, the small strain cavities were suppressed and the cavitation processes in all die drawn samples are due to the failure of the highly oriented fibrillar network caused by the breaking of the load-bearing interfibrillar/microfibrillar tie molecule chains.

1. Introduction

Semicrystalline polymers are composed of periodically stacked crystal lamellae and amorphous layers in between[1]. Various structures and the morphology of the crystals impart distinct properties to the material. Evaluating the mechanical properties of a material during deformation is crucial for determining its potential applications. Cavitation, a common phenomenon during tensile deformation, can heavily influence the appearance and properties of semicrystalline polymers. The presence of cavities sometimes results in the whitening of materials as their sizes are comparable with the wavelength of visible light[2]. Cavitation can occur at both small strains near the yield point and large strains at the late stage of tensile deformation. The appearance of

cavities at small strains is a result of a competitive process between plastic deformation of crystal lamellae and cavitation, which is dependent on the preparation of sample and test conditions[3, 4]. Galeski and his colleagues investigated the influence of deformation temperature on the cavitation of iPP during tensile deformation[4]. They found that the whitening induced by the cavities at small strains occurred only at temperatures lower than 70 °C. Song[5] studied the dependency of annealing temperature on the cavitation of iPP. It turned out that a high annealing temperature can promote this cavitation process.

Another type of cavitation occurs at large strain. At the late stage of tensile deformation, a highly oriented fibrillar structure with tie molecules connecting the adjacent fibrils/microfibrils will be formed. Upon further stretching, the entangled molecular chains may disentangle due to the breaking of the inter-microfibrillar/fibrillar tie molecules, thereby creating nucleation sites for cavities[6]. Elongated cavities with their long axis oriented along the stretching direction will appear. Peterlin[7, 8] investigated the stress whitening phenomenon resulting from cavities in fibers and highly drawn PE, iPP and nylon 66. He attributed the appearance of cavities to the crack propagation caused by the defects at the ends of micro fibrils. Recently, Lu and Men[6] studied the cavitation in isotactic polypropylene at large strains during tensile deformation. Their experiments were carried out at elevated temperatures yet below the melting temperature to suppress the occurrence of cavities in the small strain regime. They found a critical stress, depending only on the molecular weight of samples, for large strain cavitation. While numerous studies have been conducted on cavitation,

questions and controversies still arise regarding the underlying mechanisms. Hence, it is imperative to investigate the cavitation process for different activating strain regimes.

Die drawing is a widely used solid-state processing method for polymeric materials[9-11]. During the die drawing process, a heated sample billet is pulled out of a converging die by applying a pulling force on the billet at the exit side of the die. The sample is subjected to compression, shear and elongation, resulting in an increase in degree of orientation of molecular chains and a significant increase in the mechanical strength of the sample[9, 12]. After die drawing, one can occasionally observe the whitening of samples[13, 14] induced by the cavitation process during deformation. Lu[15] studied the orientation dependency of cavitation triggered at large strain in pre-oriented isotactic polypropylene samples with different molecular weight prepared by die drawing process during tensile deformation. It turned out that cavitation and final failure of samples were related not only to molecular weight but also to the preorientation. Men[16] investigated the cavitation process in β -nucleated isotactic polypropylene deformed by different solid-phase processing routes. They found that the cavitation process can be effectively suppressed in the die drawn sample. Die drawing can both diminish the number of nuclei of cavities and inhibit the growth of cavities.

Poly(4-methyl-1-pentene) (P4M1P), a linear α -polyolefin with isobutyl branches, possesses many superior advantages such as thermal stability, light weight, good release properties and optical transparency, and can be used in medical equipment, gas separation membrane production and food packaging[17-20]. Five kinds of crystal

forms of P4M1P can be obtained by various crystallization methods[21-26]. The most stable form I of P4M1P can always be obtained from the melt. The densities of the crystalline and amorphous phases in form I are almost identical. At ambient temperature the density of the crystalline phase is even slightly lower than that of the amorphous phase due to the 'interlocking' effect of large side groups in the crystals that are perpendicular to the chain axis[21]. This proximity in density between the two phases makes it difficult to determine the lamellar structure of P4M1P by small-angle X-ray scattering (SAXS) techniques, particularly at room temperature. Previous findings suggest an increase in density difference between the crystalline and amorphous phases as temperature rises[27]. The lamellar structure of P4M1P can be observed by SAXS at temperatures higher than 100 °C[28].

The ultra-small angle X-ray scattering (USAXS) technique is useful in studying the structural changes of cavities during tensile deformation since there is no interference of the scattering from the P4M1P lamellar structure. Chen and Men[29] investigated the cavitation process in P4M1P during tensile deformation at temperature below and above T_g . Their results demonstrated a two-step cavitation process that a small number of large cavities started at small strain (mode I) followed by extensively triggered small cavities at large strain (mode II). The appearance of mode II cavitation at large strains was independent of the mode I cavitation. Besides, P4M1P has a rather high melting temperature (~230 °C) and high glass transition temperature (~45 °C), which enables us to investigate the cavitation process of samples in the glassy state.

In this work we have focused on the cavitation process within die drawn P4M1P

samples during second-stage tensile deformation, both at temperatures below and above the glass transition point. To probe the structural evolution of cavities, we employed USAXS technique. We also used wide-angle X-ray diffraction (WAXD) to determine the crystalline structure, while the Halo method was employed to establish the oriented and unoriented crystalline and amorphous phases. The cavitation process in die-drawn samples is significantly affected by the deformation temperature and the initial unoriented crystalline phase during the second-stage tensile deformation in the same direction as the die drawing. The analysis of scattering and diffraction results led to better understanding of the cavitation process in pre-oriented samples.

2. Experimental section

2.1 Sample preparation

P4M1P produced by Mitsu Chemicals, Chiba, Japan with a trade name of DX845 (weight-average molecular weight (M_w) = 3.5×10^5 g mol⁻¹, number-average molecular weight (M_n) = 8.4×10^4 g mol⁻¹, polymer dispersity index (PDI) = 4.2) was used in this work. Its melting point is 232 °C and melt flow rate (MFR) is 9 g/10 min (260 °C, 5 Kg).

Sample pellets were compression molded using a hot press at 10 MPa and 280 °C into 2.0 mm films. One set of sheets were labelled as “Q” after being quenched into ice water for half an hour, while the other set were labelled as “S” after being slowly cooled to 180 °C and left for 12 hours. According to the results of Rong *et al*[30], the crystallization of P4M1P has been completed before 180 °C during the cooling process.

These two types of samples were then cut into billets with dimensions of $5 \times 2 \times 140$

mm for die-drawing experiments.

2.2 Die-drawing

The small scale die-drawing apparatus used in this work is designed and provided by the Polymer IRC laboratory at the University of Bradford (UK). The equipment incorporates a converging die with dimension of 5 mm×0.5 mm and is connected to an oven, which preheats the polymer billet. Sample billets were firstly heated to the desired temperature and then stabilized for 20 minutes. The sample Q and sample S were die drawn at a speed of 42 mm/min and temperatures of 120 °C and 150 °C. After die drawing, the sample billets were held under tension at room temperature for 20 minutes before taking them out of the die and the clamp. These die drawn samples are labeled as “Q-DD120”, “Q-DD150”, “S-DD120” and “S-DD150”, respectively. The draw ratio of die drawn sample is defined as

$$R_A = \frac{A_0}{A_F} \quad (1)$$

where A_0 and A_F are the initial cross-section area and final cross-section area of the sample and billet, respectively. The actual draw ratios of Q-DD120, Q-DD150, S-DD120 and S-DD150 are 4.75, 4.40, 5.46, 5.25, respectively.

2.3 Tensile test

After die-drawing process, strips were cut from die-drawn samples with length of 26 mm. Sample strips were further stretched at 30, 50, 70 and 90 °C with a speed of 20 $\mu\text{m/s}$ using a portable tensile testing machine (TST350, Linkam, UK). The tensile direction during second-stage deformation is the same as the die drawing direction. The deformation of P4M1P during stretching is not homogeneous due to the appearance of

necking so that the engineering strain is not applicable for a precise description of the strain dependent phenomenon. Therefore, the true strain is needed to describe the deformation of samples during stretching process. In order to measure the true strain of sample during tensile deformation, optical photographs of the deformed area were collected during stretching. In this work, the Hencky strain ε_H is used as the true strain, which is defined as

$$\varepsilon_H = 2 \ln \frac{b_0}{b} \quad (2)$$

where b_0 and b are the initial and instantaneous widths of sample during stretching process, respectively.

The true stress of sample during tensile deformation is defined as

$$\sigma_H = \frac{F}{A_0} \left(\frac{b_0}{b}\right)^2 \quad (3)$$

where F and A_0 are force and initial cross-section area of sample, respectively.

2.4 Small Angle X-ray Scattering (SAXS)

SAXS experiments were carried out on a modified Xeuss system using a Cu-K α X-ray source (GeniX3D Cu ULD, Xenocs SA, France, $\lambda = 0.154$ nm). Sample to detector distance was 2432 mm. To overcome the difficulty to obtain meaningful SAXS data due to the extremely low density difference between crystalline and amorphous phases of P4M1P at room temperature, a small piece of sample was heated up to 150 °C by a hot stage (HCS 412W, NSTEC, America) installed at the setup. Each SAXS pattern was recorded with a Pilatus 100K detector (Dectris, Swiss, 487 pixels \times 197 pixels, pixel size = 172 μ m) with an exposure time of 3600 s. All two-dimensional (2D) SAXS patterns were background corrected according to a general procedure.

2.5 *in situ* Ultra-Small Angle X-ray Scattering (USAXS)

In situ USAXS experiments were performed with the same setup as SAXS but at a sample-to-detector distance of 6490 mm, providing an effective scattering vector q ($q = (4\pi\sin\theta)/\lambda$, where 2θ is the scattering angle and λ the wavelength of the X-ray) ranging from 0.022 to 0.24 nm⁻¹. In order to investigate the structure evolution of die drawn sample during tensile deformation, a portable tensile testing machine was installed in the X-ray setup and a stepwise tension experiment was employed at a constant cross-head speed of 20 μm/s at different deformation temperatures. Each USAXS pattern was collected within 300 s and background subtracted before further analysis.

2.6 Wide Angle X-ray Diffraction (WAXD)

WAXD experiments were carried out with a customized micro-focus X-ray diffraction setup of Xenocs, France. The system uses a Cu-K_α X-ray source (GeniX3D Cu ULD, Xenocs SA, France, $\lambda = 0.154$ nm) and a focusing mirror to focus the X-rays to a spot size of 40×60 μm² at the sample position. Each WAXD pattern was collected within 120 s using also a Pilatus 100K detector. Sample to detector distance is 55.5 mm. All WAXD patterns were background corrected before further analysis.

The Halo method was used to decompose one 2D WAXD pattern into two WAXD patterns, representing the isotropic and the anisotropic diffraction signal contributions of the sample, respectively[31, 32]. The original patterns of different samples were processed by Fraser Correction[33] before using Halo method due to the distortion effect caused by the flat detector.

In order to further determine the orientation state in die-drawn samples, we also used the Hermans equation[34] to calculate the degree of orientation of molecular chains in (200) plane, which is defined as

$$S_{(hkl)} = \frac{3\langle \cos^2 \varphi_{hkl} \rangle - 1}{2} \quad (4)$$

where φ_{hkl} represents the angle between the normal direction of the (200) plane and die drawing direction. When the molecular chains are perfectly oriented along the die drawing direction, $S_{(200)} = -0.5$.

$\langle \cos^2 \varphi_{hkl} \rangle$ is obtained by equation (5)

$$\langle \cos^2 \varphi_{hkl} \rangle = \frac{\int_0^{\frac{\pi}{2}} I_{hkl}(\varphi) \sin \varphi \cos^2 \varphi d\varphi}{\int_0^{\frac{\pi}{2}} I_{hkl}(\varphi) \sin \varphi d\varphi} \quad (5)$$

where $I_{hkl}(\varphi)$ is the scattering intensity along the angle φ . φ is obtained by Polanyi equation[35]

$$\cos \varphi_{hkl} = \cos \theta_{hkl} \cos \psi \quad (6)$$

where $2\theta_{hkl}$ is the Bragg scattering angle and ψ is the azimuthal angle along the Debye circle.

2.7 Differential scanning calorimetry (DSC)

DSC measurements were conducted with a DSC1 Star[®] System (Mettler Toledo, Swiss). The virgin samples and die drawn samples were heated up from 25 °C to 280 °C under N₂ atmosphere with a heating rate of 10 K/min. The ideal value of heat fusion for 100% crystallized P4M1P to determine the weight crystallinity is 61.7 J/g[36].

3. Results and Discussion

3.1 Structural Information of the die drawn samples

Table 1. The crystallinity, long spacing, lamellar thickness and amorphous layer

thickness of different samples used in this work

Sample	Φ_c (DSC) (%)	d_{ac} (nm)	d_c (nm)	d_a (nm)
Q	50.1	27.3	13.7	13.6
S	62.9	37.0	23.2	13.8
S-DD120	58.9	25.1	14.8	10.3
S-DD150	60.6	24.2	14.7	9.5
Q-DD120	53.6	20.9	11.2	9.7
Q-DD150	53.7	21.7	11.7	10.0

Table 1 collects the long period, thickness of crystalline lamellae and amorphous layers as well as crystallinity results of different samples. The DSC heating curves of different samples are shown in Figure S1 of Supporting Information. The SAXS experiments were performed at 150 °C since the scattering intensity was too weak at room temperature due to the similar electron density of the crystalline and amorphous phases in P4M1P. The d_{ac} was derived from the position of the maximum in Lorentz corrected curve[37]. The crystallinity of the slow cooled sample is larger than that of the quenched sample. After die drawing, the crystallinity of the quenched sample increased slightly whereas the crystallinity of the slow-cooled sample decreased. The change in crystallinity is a result of both the destruction of crystals and the creation of new crystals. The crystals induced during quenching is imperfect. During the die drawing process, the crystals are annealed at high temperature and go through melting and recrystallization, resulting in an increase in crystallinity. In the case of sample S,

the deformation temperature was lower than the crystallization temperature, crystals in the sample underwent destruction during die drawing process, thus the crystallinity decreased. The thickness of the lamellae here was determined by weight crystallinity and long period for a semi-quantitative analysis because it is rather difficult to obtain accurate values of volume crystallinity of P4M1P.



Figure 1. Optical photographs of different samples. Elongation direction: horizontal.

Figure 1 illustrates optical photographs of different samples after die drawing. The transparency varied for the die-drawn samples while the samples before deformation had a similar appearance. The sample S die drawn at 120 °C exhibited a distinct whitening phenomenon and the sample S die drawn at 150 °C became slightly opaque,

whereas no evident change in appearance was observed in the two quenched samples after die drawing. The stress whitening phenomenon in semicrystalline polymers during deformation is attributed to the emergence of cavities with size comparable to the wavelength of visible light. There are two kinds of different cavitation processes in deformed semicrystalline polymer generated at small strains near yield and large strain regimes, respectively. Stress whitening that occurs in the small strain regime is highly sensitive to the testing conditions and microstructures of materials. Both high crystallinity and large lamellar thickness, as well as low stretching temperature can promote this process[38, 39]. This is due to the fact that cavitation generated near the yield point is a competitive process between plastic yielding of crystalline lamellae and cavitation[40]. The occurrence of whitening phenomenon is determined by the critical stress of cavitation and yield of crystals. Based on the structure information from Table 1 as determined by DSC and SAXS, only sample S (high crystallinity and thicker lamellae) deformed at low temperature show obvious stress whitening.

3.2 Cavitation in Die Drawn Samples during second-stage deformation

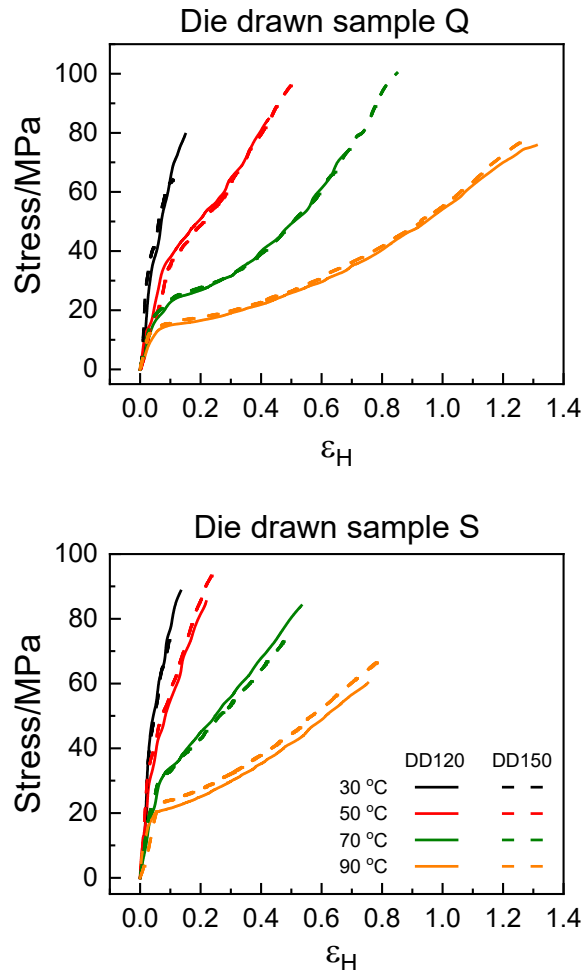


Figure 2. True stress-strain curves of different die drawn samples stretched at different temperatures (top: die drawn sample Q, bottom: die drawn sample S)

After die drawing, samples were further stretched in the same direction as die drawing at different temperatures. Figure 2 illustrates the true stress-strain curves of different die drawn samples during the second-stage tensile deformation. All the die drawn samples fractured rapidly and displayed no clear yielding during deformation when stretched at 30 °C and 50 °C. It seems that the die drawing temperature does not significantly influence the true stress-strain curves of samples during the second-stage deformation. The strain hardening was less intense in the samples stretched at higher temperature due to the higher molecular chain mobility at higher temperature.

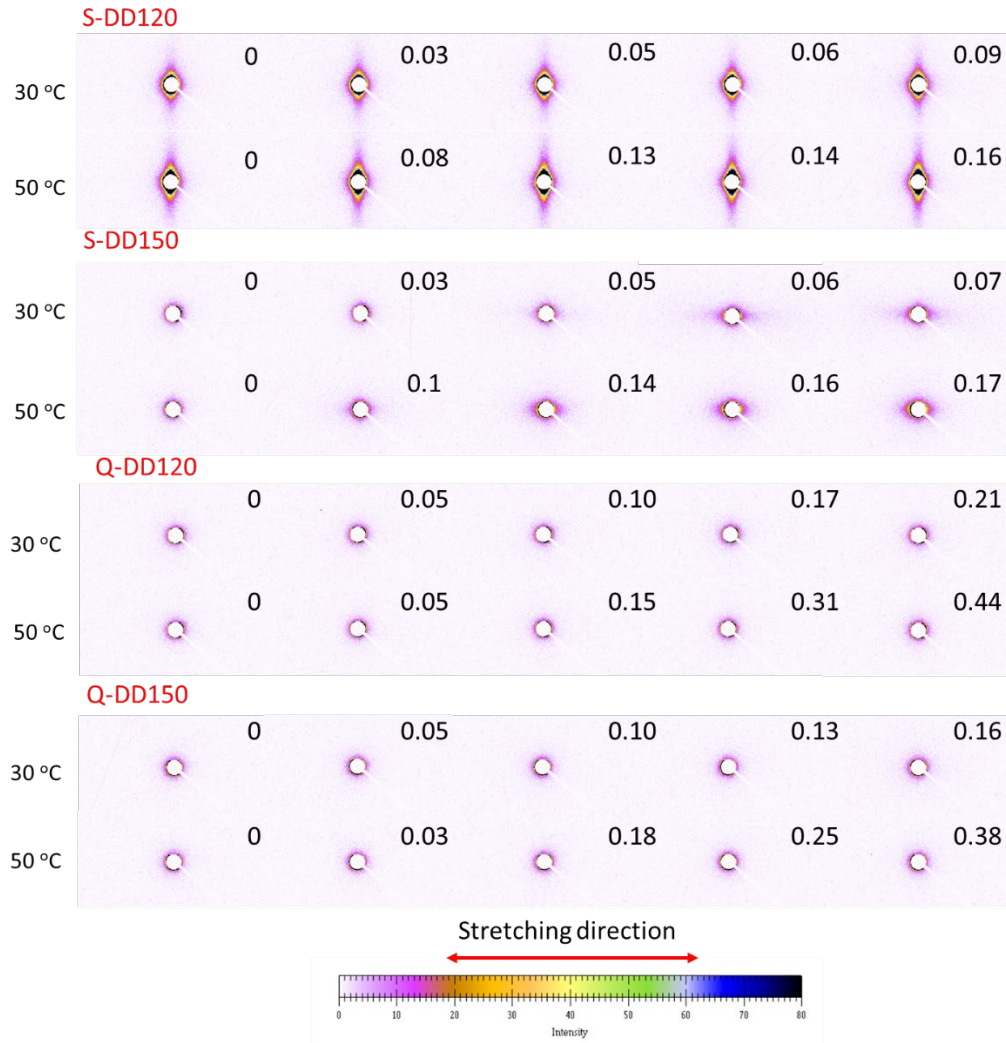


Figure 3. Selected USAXS patterns of the die-drawn samples deformed at 30 and 50 °C at different strains as indicated on the graph

In situ USAXS experiments were performed to understand the microstructure evolution of die drawn samples during the second-stage tensile deformation. Selected USAXS patterns of die drawn samples deformed at 30 °C and 50 °C are shown in Figure 3. Obvious vertical streak scattering showed up in the first pattern of S-DD120 sample. Scattering intensity in USAXS is related to the electron density difference between different scattering components in the system. The scattering signal of lamellae stacks in P4M1P is too weak to be detected at this test temperature, hence the intense scattering

streaks here can only be ascribed to structure component with large volume and large electron density contrast to the polymer matrix. Since the S-DD120 sample show clear whitening in appearance after die drawing, it is reasonable to assume that this effect is caused by cavities with size comparable to the wavelength of visible light. The long axis of cavities is parallel to the die drawing direction. Similar to the results of Lyu et al.[16], the cavities generated during the die drawing process are oriented along the deformation direction once they appear and do not adjust their orientation. During the second stage tensile deformation at 30 °C and 50 °C, the USAXS signal of S-DD120 sample show no obvious change with increasing strain.

In the case of sample S die drawn at 150 °C, the initial scattering of sample was very weak at 30 °C and 50 °C. With increasing strain, horizontal scattering streaks gradually appeared and became more and more obvious, indicating that cavities with long axis perpendicular to the stretching direction were generated during tensile deformation. The orientation of these cavities remained unchanged until the rupture of the sample.

As for the die drawn quenched sample the USAXS scattering of samples at the beginning was very weak and it did not change much during stretching at 30 °C and 50 °C. The samples did not show whitening phenomenon before fracture. This is owing to the fact that the glass transition temperature of P4M1P is about 45 °C, hence the samples are brittle at 30 °C and 50 °C. The molecular chains in sample are already oriented along the stretching direction after die drawing, with further stretching, the sample breaks before the cavities can be stabilized.

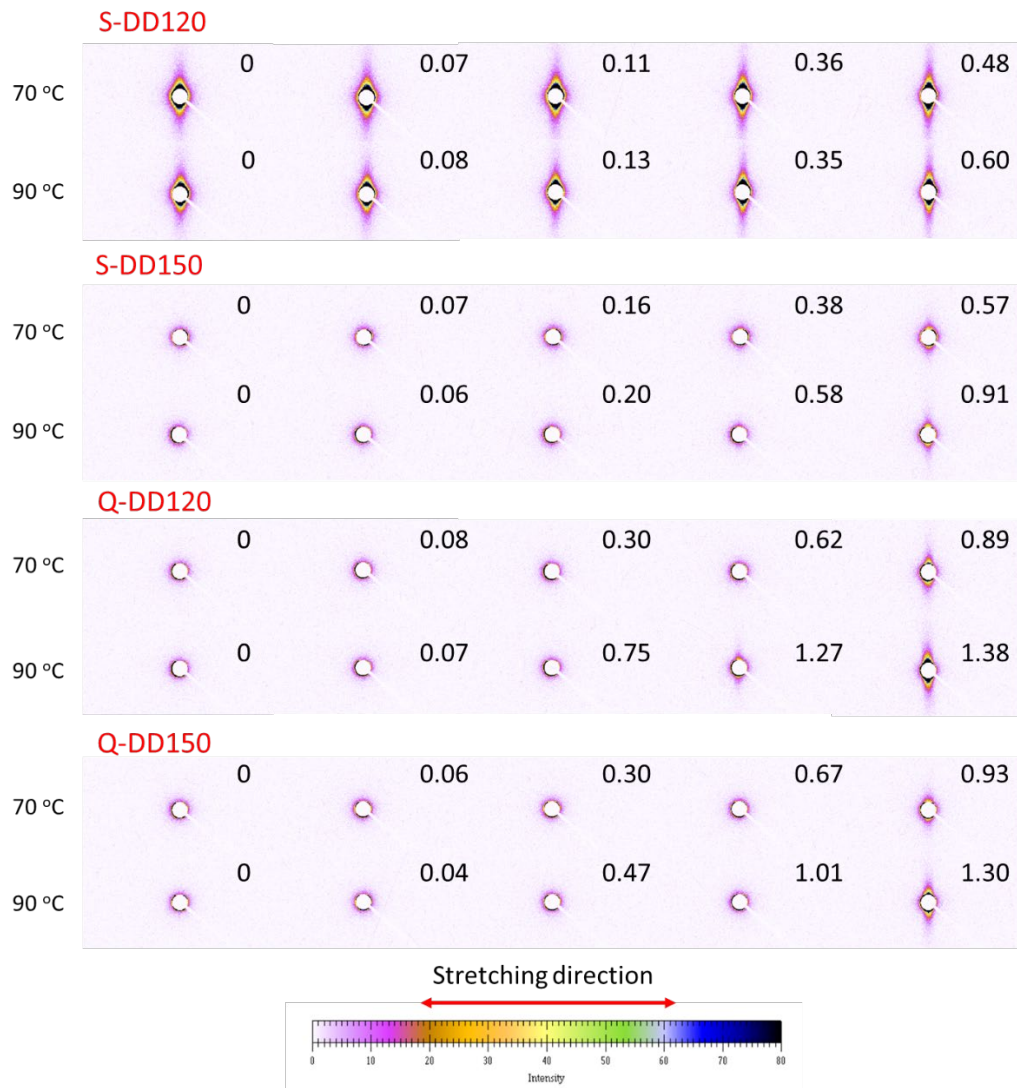


Figure 4. Selected USAXS patterns of the die-drawn samples deformed at 70 and 90 °C at different strains as indicated in the graph

Selected USAXS patterns of die drawn samples stretched at 70 °C and 90 °C are presented in Figure 4. In the case of S-DD120 sample, there was a gradual increase in intensity of scattering signal vertically as increasing strain. For the other three samples, scattering streak was not evident until the sample was close to fracturing. The samples became white as the vertical scattering streaks showed up. It should be noted that the position detected by X-ray beam was in the middle of sample strips, while the stress whitening at large strains always spreads from the edge of the sample to the center.

From the USAXS scattering data, it is evident that the whitening of the sample at high temperature is due to the presence of cavities with long axis parallel to the stretching direction. When P4M1P is stretched at temperature higher than 70 °C, the cavitation process activated around yield point is suppressed and enhanced stress-whitening shows up at large strains[41]. This phenomenon can be clarified by a well-established mechanism that the cavities formed before sample fracture result from the failure of the highly oriented amorphous network, which is initiated by breaking load-bearing interfibrillar/microfibrillar tie chains. The long axis of this kind of cavities are generally oriented along the deformation direction.

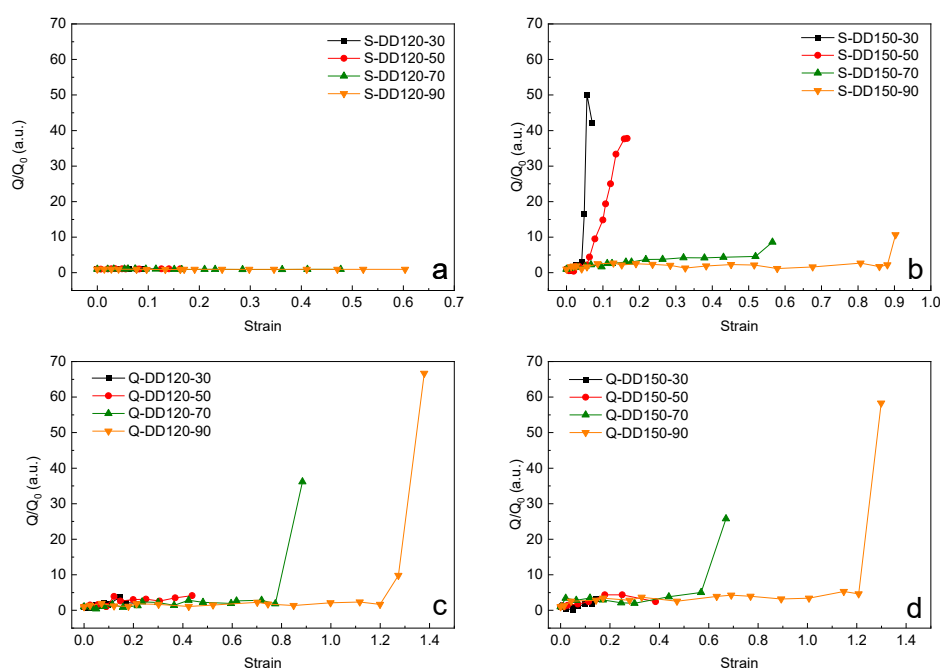


Figure 5. Relative integrated intensity obtained from USAXS patterns as a function of strain in different die drawn samples stretched at different temperatures. (a: S-DD120 b: S-DD150 c: Q-DD120 d: Q-DD150)

The integrated scattering intensity of different samples during second-stage tensile

deformation can be calculated via integrating the whole USAXS patterns. The integrated intensity Q is defined as:

$$Q \propto \int_{q_{\min}}^{q_{\max}} \int_{q_{\min}}^{q_{\max}} I(q_x, q_y) dq_x dq_y \quad (7)$$

In the case of semicrystalline polymers, Q reflects the scattering contributions of each scattered component within the system, and it is related to the volume fraction of crystalline and amorphous phases and the electron density difference between them. The variation of the samples thickness could also influence the obtained Q . To rule out the impact of the sample thickness fluctuation induced during the thermal treatment and die drawing, a relative value of integrated intensity Q/Q_0 was employed. Q and Q_0 is the integrated intensity of sample deformed to certain strain and initial die drawn sample, respectively. The calculated and corrected relative scattering intensity are summarized in Figure 5.

The scattering intensity of S-DD120 only fluctuates within a very small range compared to the other samples which show sudden and large changes in scattering intensity. Considering that cavities were already generated in this sample before the second-stage tensile deformation, further stretching may only result in the structure rearrangement of lamellar structure and existing cavities rather than forming new cavities.

When S-DD150 samples were stretched at 30 °C and 50 °C, the scattering intensity increased abruptly at small strains where whitening appears on the samples indicating the occurrence of cavities caused by the breakage of the crystalline skeleton. The gradual increase of Q/Q_0 before the sample breaks is a result of the increase of the

volume fraction of cavities in the system. At 70 °C and 90 °C, no obvious change of Q/Q_0 was observed before considerable deformation because the formation of cavities generated in the crystalline phase are suppressed at high deformation temperature. At large strains, cavities originating from the breakage of tie molecules were created in the sample thus the Q/Q_0 value increases.

For the die-drawn quenched sample, scattering intensity did not change much during the initial stage of deformation and remained so throughout the tensile process at temperatures of 30 °C and 50 °C. This suggests a rearrangement of the crystalline lamellar structure without the creation of new phases. At 70 °C and 90 °C, there was a rapid increase in the values of Q/Q_0 before sample fracture at large strains, indicating the formation of cavities.

In order to evaluate the dimension of cavities generated during the second-stage deformation, the Ruland formula[42] was used to calculate the length of long axis of cavities:

$$B_{obs} = \frac{1}{l_c} \frac{2\pi}{q} + B_{\phi} \quad (8)$$

Where B_{obs} , l_c and B_{ϕ} represent the integral breadth, the length, and the misorientation of cavities, respectively. Vertical streak scattering was used to calculate the size of cavities with their long axis parallel to the tensile direction. The calculation details are shown in the Figure S2 and Figure S3 of Supporting Information.

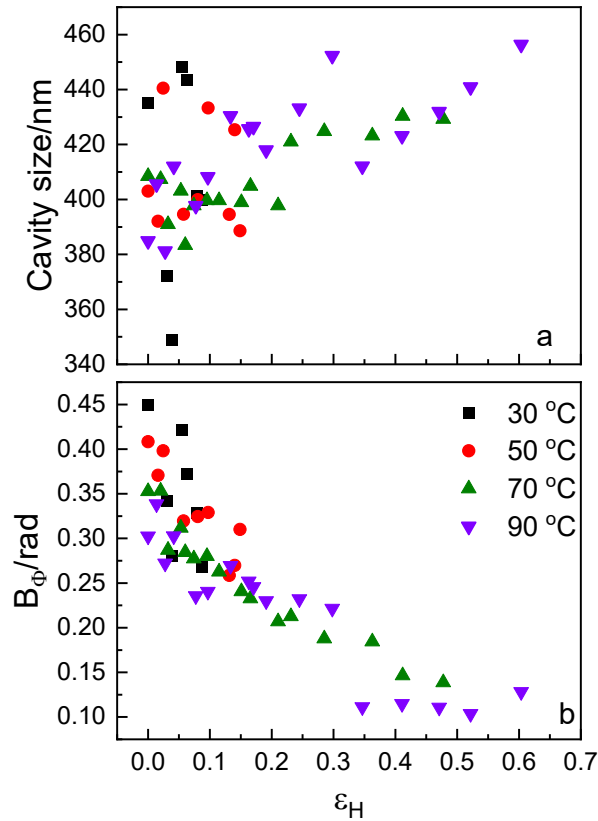


Figure 6. (a) Length of long axis and (b) misorientation of cavities obtained via Ruland method as a function of strain for S-DD120 sample stretched at different temperatures.

Figure 6 summarized the obtained results for S-DD120 sample deformed at different temperatures. At low temperature, the cavity size seems to change in a random way, but at high deformation temperature the length of cavities increases with increasing strain. The length of cavities always lies in the wavelength range of visible light. This result explains the reason why the sample becomes white during deformation. Besides, the misorientation of cavities decreases with increasing the strain, indicating that the long axis of cavities oriented more and more along stretching direction during tensile deformation.

3.3 Location of Cavities

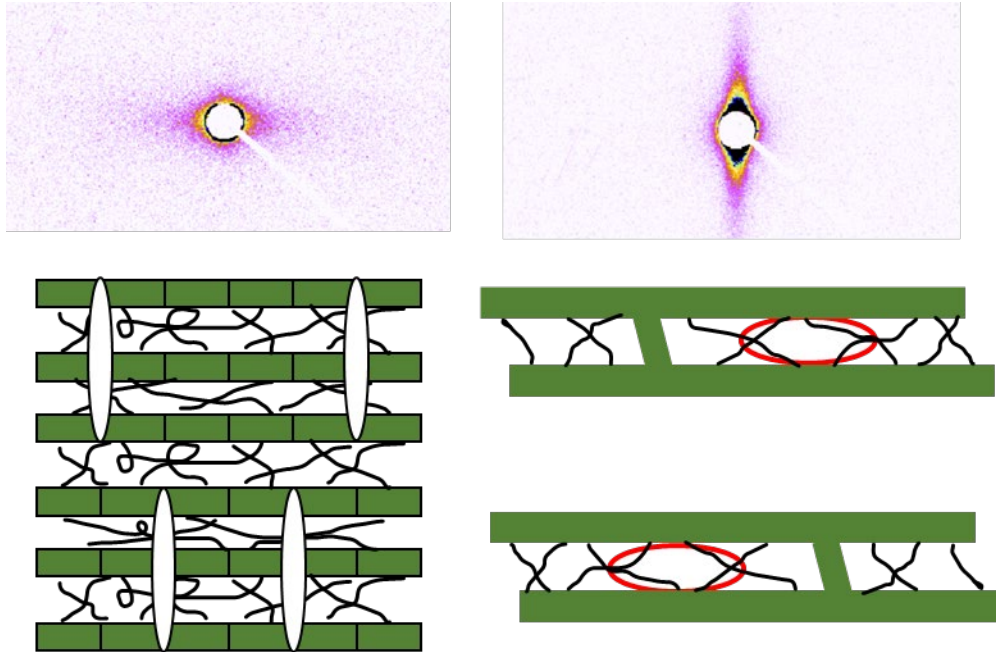


Figure 7. Schematic presentation of the formation of cavities (left: in crystalline skeleton, right: in fibrillar network. Stretching direction: horizontal)

Two types of cavities are triggered at small and large strains in deformed semi-crystalline polymers, respectively. The small strain cavitation process around the yield point originates from the crystalline skeleton at the polar region of spherulites[43]. These cavities are formed in lamellae that have normal perpendicular to the stretching direction, as shown in the Figure 7 left. When the stretching direction is perpendicular to the lamellar normal, the boundaries of crystalline blocks within lamellae open in width and cavities passing through amorphous phase are formed. Generally, the cavities generated at small strains will rearrange their direction during the tensile deformation. At the beginning, the long axis of cavities is perpendicular to the stretching direction and then parallel to the stretching direction with increasing strain. Another cavitation process occurs at large strain where fibrillar structures have been formed, as shown in

Figure 7 right. This kind of cavities is a result of rupture of the highly oriented amorphous network initiated by the breaking of interfibrillar tie chains. The long axis of these cavities created in P4M1P are usually parallel to the stretching direction.

After die drawing, the sample had experienced large deformation. Generally, the draw ratio of around 5 ($\epsilon_H \sim 1.6$) will result in a fair degree of conversion of spherulitic to fibrillar structure [9, 44]. Since the direction of second-stage tensile deformation was same as the die drawing direction, cavitation process during this stage should be due to the breaking of interfibrillar tie chains within the highly oriented amorphous network. The long axis of cavities would be oriented along the stretching deformation. However, the S-DD150 sample differs in several aspects. Cavities with long axis perpendicular to the stretching direction were still formed during the tensile deformation at 30 °C and 50 °C, indicated by the horizontal USAXAS scattering streaks. The diagrammatic sketch in Figure 7 demonstrates that the cavities resulting from the breaking of the crystalline skeleton are much easier to form when compared to the ones caused by the breaking of interfibrillar tie molecules since the long axis of these cavities are perpendicular to the stretching direction. It seems that not all crystal lamellae transformed into fibrillar structure in S-DD150 after die drawing. There were still some crystals remain unoriented within the system. These unoriented crystals create an environment suitable for the formation and stabilization of cavities with long axis perpendicular to the deformation direction.

WAXD experiments were performed to determine the molecular chains orientation of different samples after die drawing. WAXD patterns of die drawn quenched (Q) and

slow-cooled (S) samples are displayed in Figure 8. Two features can be identified in these four patterns. Firstly, oriented structures were formed both in sample Q and sample S after die drawing process, as evidenced by the concentrated diffraction signals. Secondly, the diffraction signal of lattice plane (200) of the two die-drawn quenched samples concentrated in the two spots in vertical direction, indicating that nearly all molecular chains within the crystals are aligned along the deformation direction. However, in the two die drawn sample S, the diffraction pattern of (200) crystalline lattice plane is more arc-like, particularly in the case of S-DD150 sample. The diffraction of the (200) plane is distributed throughout the entire diffraction ring, which suggests a considerable fraction of molecular chains in the crystalline phase are remained unoriented after die drawing process.

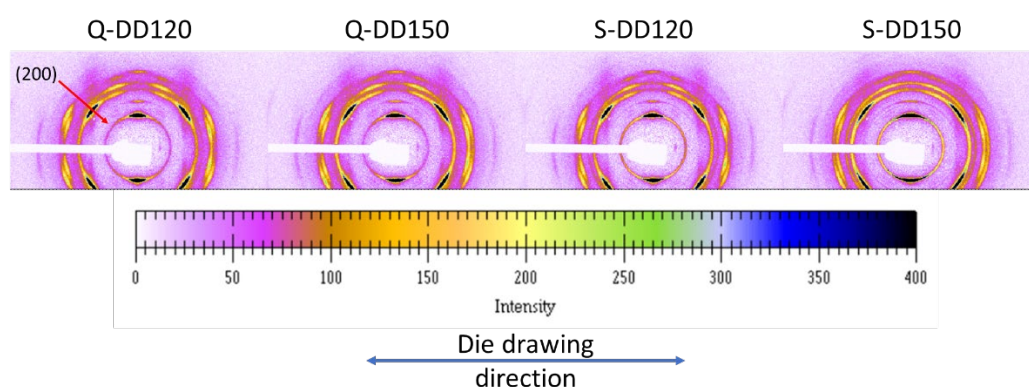


Figure 8. WAXD patterns of different die drawn samples

The WAXD pattern was split into an oriented pattern and an unoriented pattern via the Halo method[31]. By integrating both isotropic and anisotropic patterns and fitting 1D integral curves with several Gaussian peaks representing different crystallographic planes and amorphous phases, we can calculate the proportions of unoriented amorphous phase (U_a), unoriented crystalline phase (U_c), oriented amorphous phase

(O_a), and oriented crystalline phase (O_c), respectively.

Calculated results by Halo method and $S_{(200)}$ obtained by Hermans equation are collected in Table 2. Obviously, the S-DD150 sample possesses a higher proportion of unoriented crystalline phase than the other three samples and the $S_{(200)}$ of S-DD150 sample is smallest. The results in Table 2 indicate there is more lamellae with normal perpendicular to the deformation direction in the S-DD150 sample after die drawing. During the second-stage tensile deformation at 30 °C and 50 °C, block boundaries in these lamellae might open, leading to the formation of cavities with long axis perpendicular to the deformation direction. Hence, a more severe small strain cavitation behavior could be observed in the S-DD150 sample during the second-stage deformation.

Table 2. Fractions of oriented and unoriented phases obtained by Halo Method as well as the Hermans orientation factor $S_{(200)}$.

Fraction (%)	U_c	U_a	O_c	O_a	$S_{(200)}$
Q-DD120	9.1	30.5	46.8	13.6	-0.36
Q-DD150	10.5	30.4	45.6	13.5	-0.35
S-DD120	12.3	22.5	50.9	14.3	-0.34
S-DD150	17.8	23.7	47.5	11.0	-0.30

Besides, the fraction of oriented phases in the sample die drawn at high temperature is less than that of the sample die drawn at low temperature. In general,

molecular chains at high temperature are more mobile and, thus, more easily oriented under external force. Consequently, the proportion of oriented part in the sample deformed at high temperature should be higher. Nevertheless, our findings indicate otherwise. This phenomenon may be attributed to the relaxation in P4M1P. The molecular chains undergo relaxation simultaneously with orientation during deformation. Apparently, the molecular chains are more relaxed at 150 °C. Besides, the samples are softer at 150 °C so that less force was applied on the sample during the die drawing process. Both the better molecular chain relaxation and the decreased external force lead to a lower fraction of oriented crystalline phase in the sample die drawn at 150 °C compared to the one die drawn at 120 °C.

Conclusion

In summary, we have investigated the cavitation behavior in die drawn poly (4-methyl-1-pentene) samples during the second-stage tensile deformation at temperatures both below and above T_g by in situ USAXS techniques. Cavities activated at small strains around the yield point and those generated in the late stage of deformation were both observed. It turned out that the cavitation process at small strains induced by the breakage of crystalline skeleton is related to the deformation temperature and the fraction of unoriented crystalline phase in pre-oriented samples. At 30 °C and 50 °C, only sample with higher fraction of unoriented crystals showed obvious small strain cavitation. The small strain cavities oriented perpendicular to the deformation direction. At 70 °C and 90 °C, small strain cavitation was suppressed and the cavitation process

in all die drawn samples originates from the failure of the highly oriented fibrillar network caused by the breakage of interfibrillar tie chains. The long axis of cavities appeared at large strain were along the deformation direction.

Acknowledgement:

This work is supported by the National Natural Science Foundation of China (52103046), the International Partnership Program of Chinese Academy of Sciences (121522KYSB20210042) and Natural Science Foundation of Jilin Province (No. SKL202302033).

Reference

- [1] G. Strobl, *The Semicrystalline State, The Physics of Polymers: Concepts for Understanding Their Structures and Behavior*, Springer, Berlin, Heidelberg, 2007, pp. 165-222..
- [2] L. Farge, S. André, F. Meneau, J. Dillet, C. Cunat, A Common Multiscale Feature of the Deformation Mechanisms of a Semicrystalline Polymer, *Macromolecules* 46 (2013) 9659-9668.
- [3] S. Humbert, O. Lame, J.M. Chenal, C. Rochas, G. Vigier, New Insight on Initiation of Cavitation in Semicrystalline Polymers: In-Situ SAXS Measurements, *Macromolecules* 43 (2010) 7212-7221.
- [4] A. Pawlak, A. Galeski, Cavitation during tensile drawing of annealed high density polyethylene, *Polymer* 51 (2010) 5771-5779.
- [5] Y. Song, N. Nemoto, Application of an interpenetrating network model to the

necking in the microcrystalline region in four annealed isotactic polypropylene films subjected to uniaxial stretching at room temperature, *Polymer* 47 (2006) 489-497.

[6] Y. Lu, Y. Wang, R. Chen, J. Zhao, Z. Jiang, Y. Men, Cavitation in Isotactic Polypropylene at Large Strains during Tensile Deformation at Elevated Temperatures, *Macromolecules* 48 (2015) 5799-5806.

[7] A. Peterlin, Structural model of mechanical properties and failure of crystalline polymer solids with fibrous structure, *International Journal of Fracture* 11 (1975) 761-780.

[8] A. Peterlin, Plastic deformation of polymers with fibrous structure, *Colloid and Polymer Science* 253 (1975) 809-823.

[9] P.D. Coates, P. Caton-Rose, I.M. Ward, G. Thompson, Process structuring of polymers by solid phase orientation processing, *Science China Chemistry* 56 (2013) 1017-1028.

[10] P.D. Coates, I.M. Ward, Die drawing: Solid phase drawing of polymers through a converging die, *Polymer Engineering & Science* 21 (1981) 612-618.

[11] P. Wu, Q. Yang, Z. Zhao, H. Sun, T. Zhang, Y. Huang, X. Liao, Structure evolution and orientation mechanism of isotactic polypropylene during the two - stage solid die drawing process, *Journal of Applied Polymer Science* 135 (2018) 46581.

[12] J. Li, Z. Li, L. Ye, X. Zhao, P. Coates, F. Caton-Rose, M. Martyn, Structure evolution and orientation mechanism of long-chain-branched poly (lactic acid) in the process of solid die drawing, *European Polymer Journal* 90 (2017) 54-65.

[13] D. Vgenopoulos, J. Sweeney, C.A. Grant, G.P. Thompson, P.E. Spencer, P. Caton-

Rose, P.D. Coates, Nanoindentation analysis of oriented polypropylene: Influence of elastic properties in tension and compression, *Polymer* 151 (2018) 197-207.

[14] A.K. Taraiya, A. Richardson, I.M. Ward, Production and properties of highly oriented polypropylene by die drawing, *Journal of Applied Polymer Science* 33 (1987) 2559-2579.

[15] Y. Lu, G. Thompson, D. Lyu, P. Caton-Rose, P. Coates, Y. Men, Orientation direction dependency of cavitation in pre-oriented isotactic polypropylene at large strains, *Soft Matter* 14 (2018) 4432-4444.

[16] D. Lyu, Y. Sun, Y. Lu, L. Liu, R. Chen, G. Thompson, F. Caton-Rose, P. Coates, Y. Wang, Y. Men, Suppressed Cavitation in Die-Drawn Isotactic Polypropylene, *Macromolecules* 53 (2020) 4863-4873.

[17] L.C. Lopez, G.L. Wilkes, P.M. Stricklen, S.A. White, Synthesis, Structure, and Properties of Poly(4-Methyl-1 -Pentene), *Journal of Macromolecular Science Part C: Polymer Reviews* 32 (1992) 301-406.

[18] K.A. Iyer, A. Doufas, D.R. Sunagatullina, Dynamically vulcanized thermoplastic elastomers based on 4-methyl-1-pentene polymers, *Polymer* 238 (2022) 124423.

[19] M. Zhang, B. Li, J.J. Wang, H.B. Huang, L. Zhang, L.Q. Chen, Polymer Dielectrics with Simultaneous Ultrahigh Energy Density and Low Loss, *Advanced Materials* 33 (2021) 2008198.

[20] S.Y. Markova, T. Gries, V.V. Teplyakov, Poly(4-methyl-1-pentene) as a semicrystalline polymeric matrix for gas separating membranes, *Journal of Membrane Science* 598 (2020) 117754.

- [21] H. Kusanagi, M. Takase, Y. Chatani, H. Tadokoro, Crystal structure of isotactic poly(4-methyl-1-pentene), *Journal of Polymer Science: Polymer Physics Edition* 16 (1978) 131-142.
- [22] G. Charlet, G. Delmas, J.F. Revol, R.S.J. Manley, Effect of solvent on the polymorphism of poly(4-methylpentene-1): 1. Solution-grown single crystals, *Polymer* 25 (1984) 1613-1618.
- [23] J.H. Griffith, B.G. Rånby, Dilatometric measurements on poly(4-methyl-1-pentene) glass and melt transition temperatures, crystallization rates, and unusual density behavior, *Journal of Polymer Science* 44 (1960) 369-381.
- [24] C. De Rosa, Crystal Structure of Form II of Isotactic Poly(4-methyl-1-pentene), *Macromolecules* 36 (2003) 6087-6094.
- [25] S.M. Aharoni, G. Charlet, G. Delmas, Investigation of solutions and gels of poly(4-methyl-1-pentene) in cyclohexane and decalin by viscosimetry, calorimetry, and x-ray diffraction. A new crystalline form of poly(4-methyl-1-pentane) from gels, *Macromolecules* 14 (1981) 1390-1394.
- [26] R. Hasegawa, Y. Tanabe, M. Kobayashi, H. Tadokoro, A. Sawaoka, N. Kawai, Structural studies of pressure-crystallized polymers. I. Heat treatment of oriented polymers under high pressure, *Journal of Polymer Science Part A-2: Polymer Physics* 8 (1970) 1073-1087.
- [27] T. Tanigami, K. Miyasaka, Small-angle X-ray scattering of isotactic poly(4-methyl-1-pentene), *Journal of Polymer Science: Polymer Physics Edition* 19 (1981) 1865-1871.

- [28] C. Silvestre, S. Cimmino, E. Di Pace, M.L. Di Lorenzo, G. Orsello, F.E. Karasz, J.S. Lin, Morphology development of isotactic poly(4-methylpentene-1) during melt crystallization, *Journal of Materials Science* 36 (2001) 2865-2874.
- [29] R. Chen, Y. Lu, J. Zhao, Z. Jiang, Y. Men, Two - step cavitation in semi - crystalline polymer during stretching at temperature below glass transition, *Journal of Polymer Science Part B: Polymer Physics* 54 (2016) 2007-2014.
- [30] H. Bu, G. Nie, J. Rong, Crystallization and compatibility of poly(4-methyl-1-pentene) and polypropylene in their blends, *Journal of Thermoplastic Composite Materials* 28 (2013) 1110-1123.
- [31] S. Ran, X. Zong, D. Fang, B.S. Hsiao, B. Chu, R.A. Phillips, Structural and Morphological Studies of Isotactic Polypropylene Fibers during Heat/Draw Deformation by in-Situ Synchrotron SAXS/WAXD, *Macromolecules* 34 (2001) 2569-2578.
- [32] X. Yang, T. Liao, Y. Men, Structural evolution in propylene-based elastomer with γ form during stress relaxation, *Polymer* 219 (2021) 123567.
- [33] R.D.B. Fraser, T.P. Macrae, A. Miller, R.J. Rowlands, Digital processing of fibre diffraction patterns, *Journal of Applied Crystallography* 9 (1976) 81-94.
- [34] P.H. Hermans, P. Platzek, Beiträge zur Kenntnis des Deformationsmechanismus und der Feinstruktur der Hydratzellulose, *Kolloid-Zeitschrift* 88 (1939) 68-72.
- [35] M. Polanyi, Das Röntgen-Faserdiagramm, *Zeitschrift für Physik* 7 (1921) 149-180.
- [36] P. Zoller, H.W. Starkweather Jr, G.A. Jones, The heat of fusion of poly(4-methyl pentene-1), *Journal of Polymer Science Part B: Polymer Physics* 24 (1986) 1451-1458.

- [37] P. Lindner, T. Zemb, *Neutrons, X-rays and light: Scattering methods applied to soft condensed matter*, Elsevier, Amsterdam, 2002.
- [38] A. Pawlak, Cavitation during tensile deformation of isothermally crystallized polypropylene and high-density polyethylene, *Colloid and Polymer Science* 291 (2013) 773-787.
- [39] A. Pawlak, A. Galeski, Cavitation and morphological changes in polypropylene deformed at elevated temperatures, *Journal of Polymer Science Part B: Polymer Physics* 48 (2010) 1271-1280.
- [40] A. Pawlak, A. Galeski, A. Rozanski, Cavitation during deformation of semicrystalline polymers, *Progress in Polymer Science* 39 (2014) 921-958.
- [41] R. Chen, Y. Lu, Z. Jiang, Y. Men, Cavitation in Poly(4-methyl-1-pentene) during Tensile Deformation, *The Journal of Physical Chemistry B* 122 (2018) 4159-4168.
- [42] W. Ruland, Small-angle scattering studies on carbonized cellulose fibers, *Journal of Polymer Science Part C: Polymer Symposia* 28 (1969) 143-151.
- [43] Y. Men, J. Rieger, J. Homeyer, Synchrotron Ultrasmall-Angle X-ray Scattering Studies on Tensile Deformation of Poly(1-butene), *Macromolecules* 37 (2004) 9481-9488.
- [44] D. Lyu, Y. Y. Sun, Y. Q. Lai, G. Thompson, P. Caton-Rose, P. Coates, Y. Lu, Y. F. Men, Advantage of Preserving Bi-orientation Structure of Isotactic Polypropylene through Die Drawing, *Chinese Journal of Polymer Science* 39 (2021) 91-101.